Coupled dynamics of long-range and cluster-internal spin order in the cluster Mott insulator Cu_2OSeO_3

R. B. Versteeg,[1,*] J. Zhu,[1] C. Boguschewski,[1] F. Sekiguchi,[1] A. Sahasrabudhe,[1] K. Budzinauskas,[1] P. Padmanabhan,[1] P. Becker,[2] D. I. Khomskii,[1] and P. H. M. van Loosdrecht[1,†]

[1]*Institute of Physics 2, Faculty of Mathematics and Natural Sciences, University of Cologne, Zülpicher Straße 77, D-50937 Cologne, Germany*

[2]*Institute of Geology and Mineralogy, Faculty of Mathematics and Natural Sciences, University of Cologne, Zülpicher Straße 49b, D-50674 Cologne, Germany*

(Received 14 February 2019; revised manuscript received 17 May 2019; published 2 August 2019)

Cu_4 triplet clusters form the relevant spin entities for the formation of long-range magnetic order in the cluster Mott insulator Cu_2OSeO_3. Using time-resolved Raman spectroscopy, we probed photoinduced spin and lattice dynamics in this cluster magnet. Multiple picosecond-decade spin-lattice relaxation dynamics is observed, evidencing a separation of the order parameter dynamics into disordering of long-range and cluster-internal order on the tens and 100s on the picosecond timescale, respectively. We argue that this separation originates in vastly different interaction strengths between low- and high-energy spin cluster excitations and acoustic phonons. Our results exemplify the double-order parameter dynamics intrinsic to the novel quantum material class of cluster Mott insulators.

DOI: 10.1103/PhysRevB.100.064401

I. INTRODUCTION

Quantum materials with, at least, two length scales for electronic interactions lead to the self-formation of generalized molecular crystals of charge, spin, and orbital nature [1,2]. From strong shorter length scale electronic interactions, solid-state "molecules" or clusters form, which "crystallize" through weaker longer length scale electronic interactions. Such emergent solid-state molecular ground states have been identified in, for instance, the mineral Fe_3O_4 where trimeron orbital molecules form [3,4], molybdenates with triangular orbital plaquette molecules [5,6], and the honeycomb ruthenate Li_2RuO_3 with zigzag ordered singlet dimer molecules [7]. The order-to-disorder phase-transition pathways in this quantum material class, more formally known as cluster Mott insulators [8], comprises disordering of both the order inside the individual cluster actors as well as the emerging long-range cluster order. An understanding of such dynamic double-order parameter behavior is important for the fundamental understanding of electronic correlations in cluster Mott insulators and from the perspective of potential switching applications based on spin, charge, and orbital degrees of freedom [4,9,10].

In this context, we investigate the nonequilibrium dynamics of spin cluster and long-range order (LRO) in the archetypal cluster Mott insulator Cu_2OSeO_3 [11]. Nonequilibrium dynamic studies of Cu_2OSeO_3 have predominantly focused on the chiral magnetism, in particular, the manipulation and excitation of the metamagnetic Skyrmion phase [12–15]. An equally intriguing aspect of the nonequilibrium dynamics in this material concerns the disordering pathways of long-range and internal spin cluster order. The nonequilibrium dynamics is governed by lattice and spin excitations of long-range and internal cluster character and their coupling. This is expected to lead to rather rich and interesting dynamic behavior, which can be mapped in the time domain by ultrafast spectroscopy techniques [16].

The spin cluster formation in Cu_2OSeO_3 results from the geometric distortion away from a perfect magnetic pyrochlore lattice [11,17]. The magnetic unit cell is shown in Fig. 1(a) and consists of 16 Cu^{2+} $S = \frac{1}{2}$ spins on a distorted pyrochlore lattice [18]. Long and short Cu^{2+}-Cu^{2+} pathways are identified with correspondingly weak (dashed lines) and strong (full lines) exchange interactions. The $S = 1$ spin clusters form through the strong intracluster exchange interactions far above the long-range ordering temperature $T_C \approx 58$ K, below which the weak intercluster exchange interactions order the Cu_4 spin clusters into a spin cluster helix [11,19,20]. The cluster magnetic order leads to distinctly different types of low-energy (low-E) and high-energy (high-E) spin excitations with long-range and internal Cu_4 cluster character. The high-energy cluster modes can be understood as spin-flip excitations of the triplet tetrahedron as illustrated in Fig. 1(b). The collective motion of the ordered triplet clusters gives rise to spin excitations at low energy, including the Goldstone mode of the magnetically long-range-ordered state [21–23].

Time-resolved spontaneous Raman spectroscopy [24,25] allowed us to synchronously probe photoinduced spin and lattice dynamics in the spin cluster Mott insulator Cu_2OSeO_3. Multiple picosecond-decade spin-lattice relaxation dynamics is observed, revealing an efficient coupling of the high-energy spin cluster excitations to optical phonons (phs), and more importantly, that the photoinduced magnetization dynamics is governed by a double-order parameter behavior reflecting both the disordering of long-range and the internal spin cluster

*Corresponding author: versteeg@ph2.uni-koeln.de
†Corresponding author: pvl@ph2.uni-koeln.de

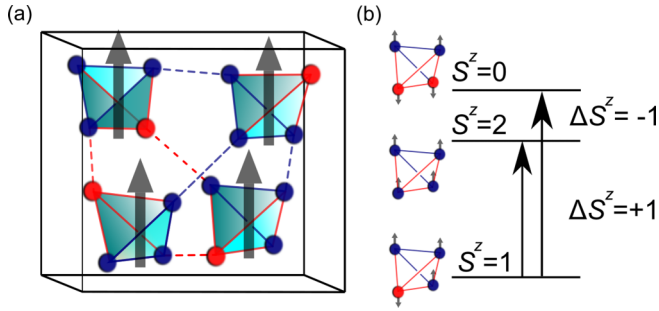

FIG. 1. (a) The magnetic unit cell of Cu_2OSeO_3. The red (spin-down) and blue (spin-up) Cu^{2+} $S = \frac{1}{2}$ spins reside on a distorted pyrochlore lattice. The exchange paths can be classified into strong (full lines) and weak (dashed line) exchange couplings. The blue lines represent a predominantly ferromagnetic exchange, whereas the red lines correspond to a predominantly antiferromagnetic exchange. The three-up-one-down spin triplet ($S = 1$) clusters are indicated in light blue with spin in gray. (b) Spin-flip excitations of a triplet tetrahedron. The spin flip leads to a rise or lowering of the cluster's total magnetic quantum number S^z.

order. Our results illustrate the double-order parameter dynamics intrinsic to cluster Mott insulator materials.

II. EQUILIBRIUM INELASTIC LIGHT-SCATTERING SPECTRUM

Before turning to the nonequilibrium optical spectroscopy results, we discuss the equilibrium inelastic light-scattering response of Cu_2OSeO_3. Single crystals of a few mm^3 size were synthesized by chemical transport reaction growth [26]. A (111)-oriented plate-shaped sample with a flat as-grown face was used. The Raman probing is realized with 2.42-eV pulses of $\Delta\nu \approx 1.2$ meV ($\approx 10\ cm^{-1}$) bandwidth [full width at half maximum (FWHM)] and $\Delta\tau \approx 1.5$ ps (FWHM) duration. The probe beam polarization is parallel to the crystallographic [$1\bar{1}0$] axis. The probing is carried out in an unpolarized Raman geometry in order to optimize the scattered light detection efficiency. The energy resolution typically lies around $10\ cm^{-1}$ and is largely dictated by the probe pulse bandwidth (see the Supplemental Material [27]).

Figure 2 shows the steady-state Raman spectra at temperatures ranging from 5 to 75 K. The large amount of atoms in the structural unit cell results in a rich set of phonon modes as indicated with an asterisk (*) in the figure [28–30]. Multiple strongly temperature-dependent modes are observed, of which two were previously assigned to $\Delta S^z = +1 (\hbar\Omega \sim 32\text{-meV})$ and $\Delta S^z = -1$ ($\hbar\Omega \sim 53$-meV) high-energy spin cluster excitations at the center of the Brillouin zone [21–23]. For these modes, which are Raman active through the Elliot-Loudon-scattering mechanism [31,32], a spectral weight (SW) transfer to lower Stokes shift Ω is observed when the temperature increases towards T_C as indicated with the gray arrows. The magnetic spectral weight transfer is understood as a softening and broadening of the $\Delta S^z = \pm 1$ spin excitations. Above $T_C \approx 58$ K, magnetic scattering still persists, however, as a broad scattering continuum [30]. Similar critical behavior was observed for a spin cluster transition in the terahertz range of the absorption spectrum [33]. The $\hbar\Omega \sim 50$- and $\hbar\Omega \sim 55$-meV modes have previously been identified as phonons [28–30]. The stronger than normal temperature sensitivity may evidence magnetoelastic coupling [34,35], in particular, in view of the proximity of the high-energy spin excitation.

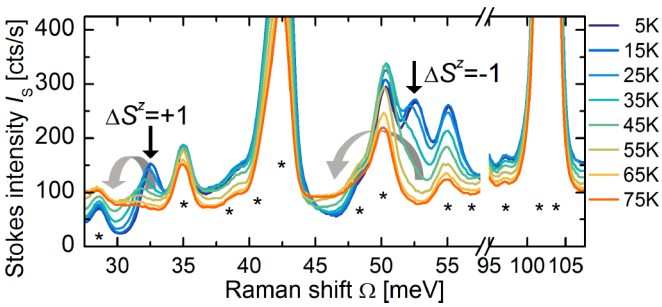

FIG. 2. Temperature-dependent steady-state Raman spectra. The modes indicated with an asterisk (*) are phonons or not fully resolved phonon regions. High-energy spin cluster excitations are observed at $\hbar\Omega \sim 32$ meV ($\Delta S^z = +1$) and $\hbar\Omega \sim 53$ meV ($\Delta S^z = -1$).

The conceptual picture of spin cluster excitations indicated in Fig. 1(b) applies well above T_C where no long-range order exists between the clusters. In this limit the high-energy spin excitations can be regarded as localized internal spin cluster excitations with a resultingly broad continuum light-scattering spectrum [30,36]. In the long-range-ordered phase, these internal cluster modes acquire dispersion by the intercluster exchange interactions and form optical magnon branches, resulting in well-defined magnetic modes in the Raman spectrum [23,37]. The Raman-active high-energy $\Delta S^z = \pm 1$ spin excitations, thus, form an optical probe for both the long-range and the internal spin cluster order below T_C. We note here that the low-energy spin excitations (<13 meV) [21,23], corresponding to the collective motion of the ordered triplet clusters, are of too low energy to be resolvable with the broadband probe pulse used as the Raman excitation source.

III. PHOTOINDUCED SPIN AND LATTICE DYNAMICS

We now turn to the optically induced spin and lattice dynamics. The Cu_2OSeO_3 sample, cooled to 5 K, is excited in the crystal-field excitation region [38] with 2.18-eV pump pulses of $\Delta\tau \approx 0.3$ ps (FWHM) duration at a fluence of $F \approx 2\ mJ/cm^2$. Note that these localized electronic excitations lie below the charge-transfer gap [38]. The fraction of photoexcited Cu^{2+} sites per pulse lies around $\sim 5 \times 10^{-6}$. The weak pump-excitation conditions ensure that we probe the near-equilibrium dynamics of the helimagnetic phase. The thermalization of the system is measured by the time evolution of the Stokes spectrum (see the Supplemental Material [27]). The Raman-probe pulse falls in the low-energy tail of the charge-transfer excitation region [38]. The Stokes Raman-scattering intensity $I_S(\Omega)$ is proportional to $I_S(\Omega) \propto V_{probe}[\alpha(\omega)]\chi_R^2(\Omega)[n(\Omega)+1]$ (Ref. [39]). Here, $V_{probe}[\alpha(\omega)]$ describes the probe volume term, which depends on the absorption coefficient $\alpha(\omega)$ at the scattered photon frequency ω. $\chi_R^2(\Omega)$ gives the squared Raman tensor, and $[n(\Omega)+1]$ gives the population factor. Under the weak pump excitation conditions, the (transient) occupation number $n(\Omega) \ll 1$ and can, thus, be neglected, i.e., $I_S(\Omega) \propto V_{probe}[\alpha(\omega)]\chi_R^2(\Omega)$.

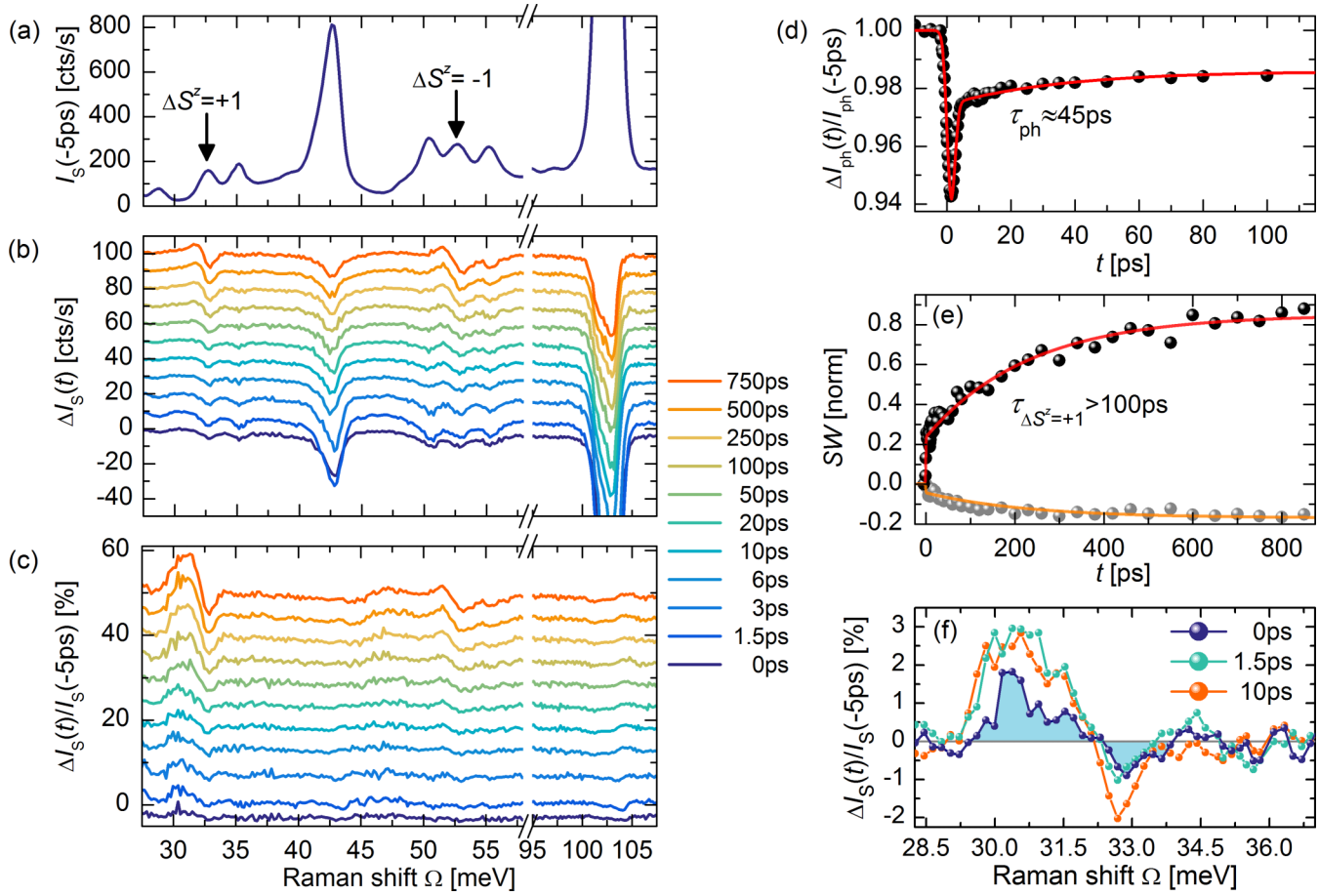

FIG. 3. (a) Stokes spectrum at 5 K. The spin cluster excitations are indicated with arrows. The other peaks are phonons. (b) Differential Stokes spectra for indicated time delays. The phonon modes show a reduction in scattering efficiency, which does not fully recover within the measured time window. The $\Delta S^z = \pm 1$ spin excitations show a dynamic softening and broadening. (c) Scaled differential spectra. From these spectra, it becomes clear that the phonons only show a negligible frequency shift, in sharp contrast with the $\Delta S^z = \pm 1$ spin excitations. After $t > 100$ ps, the spin excitation spectral weight transfer keeps on increasing. (d) $\Delta I_{\rm ph}(t)/I_{\rm ph}(-5\ {\rm ps})$ transient for the 103-meV phonon region. An initial scattering reduction and partial recovery within the time resolution is observed in addition to a longer timescale recovery. Global fitting approximately gives the same long recovery time constant of $\tau_{\rm ph} \sim 45$ ps for all phonons. (e) The softening of the $\Delta S^z = +1$ spin excitation occurs on a significantly slower timescale of $\tau_{\Delta S^z=\pm 1} > 100$ ps. Plotted is the increasing (black dots) and decreasing (gray dots) component of the spectral weight transfer. (f) Differential Stokes spectra $\Delta I_{\rm S}(\Omega, t)/I_{\rm S}(\Omega, -5\ {\rm ps})$ of the $\Delta S^z = +1$ excitation at early delay times. At pump-probe overlap ($t = 0$ ps), a spectral weight shift is established, revealing an efficient energy relaxation channel on the shortest timescale (<1.5 ps).

In Fig. 3, we show our main result: the transient evolution of the Stokes spectrum $I_{\rm S}(\Omega, t)$, where t refers to the pulse delay time and Ω refers to the Stokes shift. For clarity the pre-time-zero Stokes spectrum $I_{\rm S}(\Omega, -5\ {\rm ps})$ is plotted in Fig. 3(a). Figures 3(b) and 3(c) show the differential Stokes spectra $\Delta I_{\rm S}(\Omega, t) = I_{\rm S}(\Omega, t)/I_{\rm S}(\Omega, -5\ {\rm ps})$ and scaled differential Stokes spectra $\Delta I_{\rm S}(\Omega, t)/I_{\rm S}(\Omega, -5\ {\rm ps})$ for the time delays indicated in the figure. The two main observations are a decrease with subsequent recovery of the phonon-scattering intensity and a transient broadening and spectral weight transfer to lower Ω of the $\Delta S^z = \pm 1$ spin excitations. Similar behavior is observed at higher bias temperatures.

The scattering intensity of selected ph modes is integrated over a range of $\sim 3 \times$ FWHM centered at the phonon energy to give $I_{\rm ph}(t)$ and shown in Fig. 3(d) as relative transient phonon-scattering intensity $\Delta I_{\rm ph}(t)/I_{\rm ph}(-5\ {\rm ps})$. For all phonons, an initial Stokes-scattering efficiency decrease of $\sim$5% after excitation is observed with a partial recovery within the temporal pump-probe pulse overlap. A slower recovery timescale of $\tau_{\rm ph} \sim 45$ ps is observed to $\Delta I_{\rm ph}(t)/I_{\rm ph}(-5\ {\rm ps}) \approx -1.5\%$ at late delay times. The phonon spectral shape hardly changes as most clearly seen in the scaled differential Stokes spectra [Fig. 3(c)]. From these observations, it becomes apparent that the Raman spectra show an overall reduction and recovery in scattering efficiency due to a transient change in absorption with a concomitant change in $V_{\rm probe}[\alpha(\omega)]$.

A transient softening and broadening of the $\Delta S^z = \pm 1$ spin excitation scattering is observed due to excitation of the magnetic system. Note that the asymmetric line shape in the (scaled) differential spectra originates from a line-shape change in $\chi_{\rm R}^2(\Omega)$ and not from the population term $n(\Omega)$. The time-dependent dynamics of the spin excitation scattering is convoluted with the change in the probing volume. This effect is deconvoluted by scaling the spectrum with the scattering

intensity of the phonon response, giving the intensity ratio,

$$\frac{I_{\Delta S^z=\pm1}}{I_{\rm ph}} \propto \frac{\chi^2_{\Delta S^z=\pm1}}{\chi^2_{\rm ph}}. \quad (1)$$

The intensity ratio is integrated over the increasing and decreasing scattering spectral component (integration ranges of 28.5–32.3 and 32.7–33.5 meV, respectively) to give a SW function of the high-energy spin excitation scattering as plotted for $\Delta S^z = +1$ in Fig. 3(e). A stepwise ($\tau < 1.5$-ps) SW transfer is observed, followed by a $\tau_{\Delta S^z=\pm1} > 100$-ps spin-lattice relaxation component. A zoom in on the early timescale spectral dynamics of the $\Delta S^z = +1$ excitation is plotted in Fig. 3(f). The SW transfer at $t = 0$ and $t = 1.5$ ps amounts to about 15%–30%, respectively, of the SW transfer at late time-delays t. This evidences an efficient ultrafast spin disordering mechanism, in agreement with the observations described in Ref. [14]. Similar dynamics is observed for the $\Delta S^z = -1$ excitation (see the Supplemental Material [40]). Comparison of the $\Delta S^z = +1$ spin excitation peak shift at late delay times with steady-state data allows to calculate a heating of $\Delta T \approx 7$ K when quasiequilibrium is established, in good agreement with the temperature increase estimated from the pulse power, absorption coefficient [38], and low-temperature heat capacity of Cu_2OSeO_3 [20,41].

The disordering of long-range and internal spin cluster order occurs through different spin-lattice relaxation channels [10,42,43]. After the optical excitation, the electronically excited system dissipates energy by emission of optical phonons, which, subsequently, decay into acoustic phonons [44–46]. These relaxation processes take place within a few picoseconds as evidenced from the fast overall scattering reduction and recovery taking place within the temporal pump-probe overlap. The rapid magnetic spectral weight transfer [Figs. 3(e) to 3(f)] on the shortest timescale is evidence of an additional decay mechanism for the optical phonons into high-energy spin cluster excitations, which leads to an ultrafast reduction of long-range and internal spin cluster order. Such efficient phonon-magnon decay is enabled by the energy-momentum-dispersion overlap of the optical phonons and the high-energy spin cluster excitations [23,42].

The separation between long-range and internal spin cluster order dynamics becomes apparent over longer timescales. The long timescale spin-lattice equilibration is microscopically dictated by the coupling between acoustic phonons and low- and high-energy spin cluster excitations [43]. The recovery timescale $\tau_{\rm ph} \sim 45$ ps is too slow for optical to acoustic phonon decay [44–46]. In magnetic insulators, these longer timescales are typical for spin-lattice-driven demagnetization [45]. We, therefore, assign the 45-ps timescale to the decay of acoustic phonons into low-energy and high-energy spin excitations. The high-energy spin excitations show a substantially longer thermalization timescale of $\tau_{\Delta S^z=\pm1} > 100$ ps. The low-energy cluster excitation thermalization dynamics can be obtained by fitting a phenomenological three-temperature model [10] to the phonon and high-energy spin excitation transients as shown in Fig. 4. The change in the acoustic phonon temperature is proportional to the change in the phonon Raman-scattering intensity. The change in the high-energy spin excitation temperature is proportional

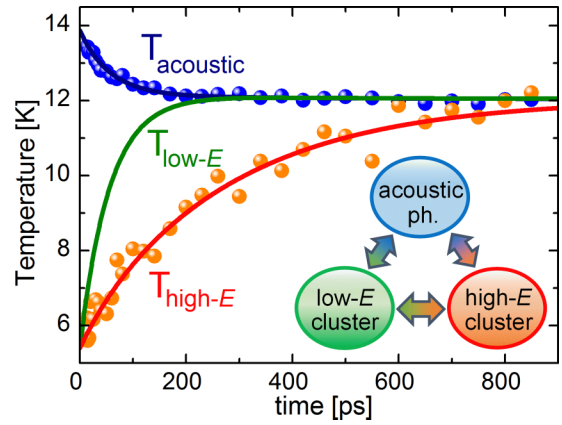

FIG. 4. Acoustic ph, low-E, and high-E spin excitation equilibration dynamics after $t > 6$ ps. Effective temperatures are indicated with $T_{\rm acoustic}$ for the acoustic phonons and $T_{\text{low-}E}$ and $T_{\text{high-}E}$ for the low-energy and high-energy spin cluster excitations.

to the observed spin excitation spectral weight transfer. The solid lines are the solution to the three-temperature model [41] (see the Supplemental Material [47]). A long-range disordering time of $\tau_{\rm LRO} \sim 55$ ps is found from the low-energy spin excitation thermalization. The high-energy spin excitations form a dual probe of long-range and internal spin cluster order. From the high-energy spin excitation thermalization, we infer an internal cluster disordering time of $\tau_{\rm cluster} \sim 400$ ps. Similar demagnetization timescales were reported in Ref. [14].

The separation into double magnetic order parameter dynamics is understood from vastly different phonon-magnon interactions. Acoustic phonons couple strongly to the low-energy spin cluster excitations [35] but only weakly to the high-energy spin cluster excitations [42]. Phonon decay into low-energy spin excitations of the long-range-ordered state describes the conventional demagnetization pathway of insulating magnetic materials [10,43]. The disordering of internal spin cluster order, however, has to occur through up-conversion of acoustic phonons and/or low-energy spin

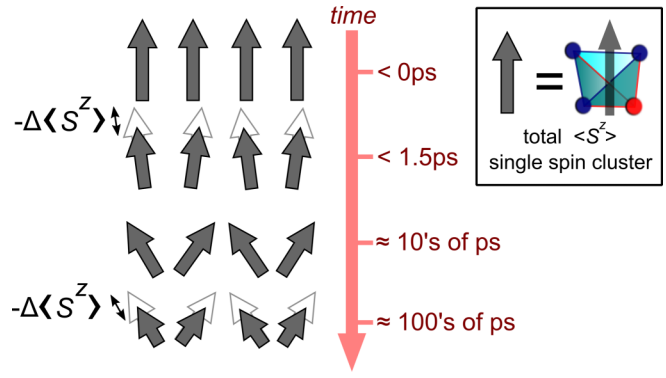

FIG. 5. Summary of the photoinduced multiple picosecond-decade spin disordering dynamics. The total spin length $\langle S^z \rangle$ of a single spin cluster is indicated with a gray arrow. The disordering of internal spin cluster order is depicted as a $-\Delta\langle S^z \rangle$ spin length reduction. Long-range disordering is depicted by a reorientation of the cluster spins.

excitations into high-energy spin cluster excitations, forming a scattering bottleneck in the equilibration dynamics.

The multiple picosecond-decade long-range and internal spin cluster order parameter dynamics is summarized in Fig. 5. An initial ultrafast ($\tau < 1.5$-ps) reduction of long-range and internal spin cluster order results from the decay of optical phonons into high-energy spin cluster excitations. This is depicted by a disordering of the cluster spin alignment and a $-\Delta\langle S^z\rangle$ decrease in spin length for the clusters. On the tens of picosecond timescale, the long-range ordering of spin clusters decreases by decay of acoustic phonons into low-energy spin excitations. On the 100s of picosecond timescale, the internal spin cluster order decreases through up-conversion of acoustic phonons and/or low-energy spin excitations into high-energy spin cluster excitations.

IV. CONCLUSIONS

We have studied the photoinduced disordering of long-range and internal spin cluster order in the spin cluster Mott insulator Cu_2OSeO_3 using time-resolved Raman spectroscopy as a selective probe for spin and lattice dynamics. Multiple picosecond-decade dynamics were observed, evidencing a separation of the order parameter dynamics into disordering of long-range order on the tens of picosecond timescale and disordering of internal spin cluster order on the 100s of picosecond timescale. This separation was discussed in terms of vastly different interaction strengths between low- and high-energy spin excitations and acoustic phonons. Our results provide new insight on the photoinduced nonequilibrium dynamics in the cluster magnet Cu_2OSeO_3 and exemplify the double-order parameter dynamics of generalized molecular crystals of charge, spin, and orbital nature. Double-order parameter dynamics is not only important in the context of cluster magnets, such as Cu_2OSeO_3, but also may be of relevance in addressing current problems in the broader class of cluster Mott insulators, such as unraveling the nature and speed limit of phase transitions in materials with orbital or charge molecules [4,9] and destabilization of spin-dimer or charge-localization competing phases in spin liquid candidate materials [48,49].

ACKNOWLEDGMENTS

This project was partially financed by the Deutsche Forschungsgemeinschaft (DFG) through SFB Grossgeräteantrag Grant No. INST217/782-1 and SFB-1238 (Projects No. A02 and No. B05). R.B.V. acknowledges funding through the Bonn-Cologne Graduate School of Physics and Astronomy (BCGS). R.B.V. thanks D. Inosov (Dresden, DE), S. Diehl (Cologne, DE), C. Kollath (Bonn, DE), and F. Parmigiani (Trieste, IT) for fruitful discussions.

[1] J. P. Attfield, Orbital molecules in electronic materials, APL Mater. **3**, 041510 (2015).

[2] S. V. Streltsov and D. I. Khomskii, Orbital physics in transition metal compounds: New trends, Phys.-Usp. **60**, 1121 (2017).

[3] M. S. Senn, J. P. Wright, and J. P. Attfield, Charge order and three-site distortions in the Verwey structure of magnetite, Nature (London) **481**, 173 (2012).

[4] S. de Jong, R. Kukreja, C. Trabant, N. Pontius, C. F. Chang, T. Kachel, M. Beye, F. Sorgenfrei, C. H. Back, B. Bräuer, W. F. Schlotter, J. J. Turner, O. Krupin, M. Doehler, D. Zhu, M. A. Hossain, A. O. Scherz, D. Fausti, F. Novelli, M. Esposito, W. S. Lee, Y.-D. Chuang, D. H. Lu, R. G. Moore, M. Yi, M. Trigo, P. Kirchmann, L. Pathey, M. S. Golden, M. Buchholz, P. Metcalf, F. Parmigiani, W. Wurth, A. Föhlisch, C. Schüßler-Langeheine, and H. A. Dürr, Speed limit of the insulator-metal transition in magnetite, Nat. Mater. **12**, 882 (2013).

[5] J. P. Sheckelton, J. R. Neilson, D. G. Soltan, and T. M. McQueen, Possible valence-bond condensation in the frustrated cluster magnet $LiZn_2Mo_3O_8$, Nat. Mater. **11**, 493 (2012).

[6] W. H. McCarroll, L. Katz, and R. Ward, Some ternary oxides of tetravalent molybdenum, J. Am. Chem. Soc. **79**, 5410 (1957)

[7] Y. Miura, M. Sato, Y. Yamakawa, T. Habaguchi, and Y. Ono, Structural transition of Li_2RuO_3 induced by molecular-orbit formation, J. Phys. Soc. Jpn. **78**, 094706 (2009).

[8] G. Chen and P. A. Lee, Emergent orbitals in the cluster Mott insulator on a breathing kagome lattice, Phys. Rev. B **97**, 035124 (2018).

[9] S. Wall, S. Yang, L. Vidas, M. Chollet, J. M. Glownia, M. Kozina, T. Katayama, T. Henighan, M. Jiang, T. A. Miller, D. A. Reis, L. A. Boatner, O. Delaire, and M. Trigo, Ultrafast disordering of vanadium dimers in photoexcited VO_2, Science **362**, 572 (2018).

[10] A. Kirilyuk, A. V. Kimel, and T. Rasing, Ultrafast optical manipulation of magnetic order, Rev. Mod. Phys. **82**, 2731 (2010).

[11] O. Janson, I. Rousochatzakis, A. A. Tsirlin, M. Belesi, A. A. Leonov, U. K. Rößler, J. Van den Brink, and H. Rosner, The quantum nature of skyrmions and half-skyrmions in Cu_2OSeO_3, Nat. Commun. **5**, 5376 (2014).

[12] S. Seki, X. Z. Yu, S. Ishiwata, and Y. Tokura, Observation of skyrmions in a multiferroic material, Science **336**, 198 (2012).

[13] N. Ogawa, S. Seki, and Y. Tokura, Ultrafast optical excitation of magnetic skyrmions, Sci. Rep. **5**, 9552 (2015).

[14] M. C. Langner, S. Roy, S. W. Huang, J. D. Koralek, Y.-D. Chuang, G. L. Dakovski, J. J. Turner, J. S. Robinson, R. N. Coffee, M. P. Minitti, S. Seki, Y. Tokura, and R. W. Schoenlein, Nonlinear Ultrafast Spin Scattering in the Skyrmion Phase of Cu_2OSeO_3, Phys. Rev. Lett. **119**, 107204 (2017).

[15] J. S. White, I. Živković, A. J. Kruchkov, M. Bartkowiak, A. Magrez, and H. M. Rønnow, Electric-Field-Driven Topological Phase Switching and Skyrmion-Lattice Metastability in Magnetoelectric Cu_2OSeO_3, Phys. Rev. Appl. **10**, 014021 (2018).

[16] J. Orenstein, Ultrafast spectroscopy of quantum materials, Phys. Today **65**(9), 44 (2012).

[17] J. M. Hopkinson and H.-Y. Kee, Geometric frustration inherent to the trillium lattice, a sublattice of the B20 structure, Phys. Rev. B **74**, 224441 (2006).

[18] J.-W. G. Bos, C. V. Colin, and T. T. M. Palstra, Magnetoelectric coupling in the cubic ferrimagnet Cu_2OSeO_3, Phys. Rev. B **78**, 094416 (2008).

[19] G. S. Tucker, J. S. White, J. Romhányi, D. Szaller, I. Kézsmárki, B. Roessli, U. Stuhr, A. Magrez, F. Groitl, P. Babkevich, P. Huang, I. Živković, and H. M. Rønnow, Spin excitations in the skyrmion host Cu_2OSeO_3, Phys. Rev. B **93**, 054401 (2016).

[20] T. Adams, A. Chacon, M. Wagner, A. Bauer, G. Brandl, B. Pedersen, H. Berger, P. Lemmens, and C. Pfleiderer, Long-wavelength Helimagnetic Order and Skyrmion Lattice Phase in Cu_2OSeO_3, Phys. Rev. Lett. **108**, 237204 (2012).

[21] J. Romhányi, J. van den Brink, and I. Rousochatzakis, Entangled tetrahedron ground state and excitations of the magnetoelectric skyrmion material Cu_2OSeO_3, Phys. Rev. B **90**, 140404(R) (2014).

[22] M. Ozerov, J. Romhányi, M. Belesi, H. Berger, J.-P. Ansermet, J. van den Brink, J. Wosnitza, S. A. Zvyagin, and I. Rousochatzakis, Establishing the Fundamental Magnetic Interactions in the Chiral Skyrmionic Mott Insulator Cu_2OSeO_3 by Terahertz Electron Spin Resonance, Phys. Rev. Lett. **113**, 157205 (2014).

[23] P. Y. Portnichenko, J. Romhányi, Y. A. Onykiienko, A. Henschel, M. Schmidt, A. S. Cameron, M. A. Surmach, J. A. Lim, J. T. Park, A. Schneidewind, D. L. Abernathy, H. Rosner, J. van den Brink, and D. Inosov, Magnon spectrum of the helimagnetic insulator Cu_2OSeO_3, Nat. Commun. **7**, 10725 (2016).

[24] R. B. Versteeg, J. Zhu, P. Padmanabhan, C. Boguschewski, R. German, M. Goedecke, P. Becker, and P. H. M. van Loosdrecht, A tunable time-resolved spontaneous Raman spectroscopy setup for probing ultrafast collective excitation and quasiparticle dynamics in quantum materials, Struct. Dyn. **5**, 044301 (2018).

[25] D. Fausti and P. H. M. van Loosdrecht, in *Optical Techniques for Solid-State Materials Characterization*, edited by R. P. Prasankumar and A. J. Taylor (CRC, Boca Raton/London/New York, 2012).

[26] M. Belesi, I. Rousochatzakis, H. C. Wu, H. Berger, I. V. Shvets, F. Mila, and J.-P. Ansermet, Ferrimagnetism of the magnetoelectric compound Cu_2OSeO_3 probed by ^{77}SeNMR, Phys. Rev. B **82**, 094422 (2010).

[27] See Supplemental Material at http://link.aps.org/supplemental/10.1103/PhysRevB.100.064401 for more details on the (time-resolved) spontaneous Raman spectroscopy experiment.

[28] V. P. Gnezdilov, K. V. Lamonova, Y. G. Pashkevich, P. Lemmens, H. Berger, F. Bussy, and S. L. Gnatchenko, Magnetoelectricity in the ferrimagnetic Cu_2OSeO_3: Symmetry analysis and Raman scattering study, Low Temp. Phys. **36**, 550 (2010).

[29] K. H. Miller, X. S. Xu, H. Berger, E. S. Knowles, D. J. Arenas, M. W. Meisel, and D. B. Tanner, Magnetodielectric coupling of infrared phonons in single-crystal Cu_2OSeO_3, Phys. Rev. B **82**, 144107 (2010).

[30] V. S. Kurnosov, V. P. Gnezdilov, V. V. Tsapenko, P. Lemmens, and H. Berger, Analysis of the low-frequency spectrum of the cubic noncentrosymmetric ferrimagnet Cu_2OSeO_3, Low Temp. Phys. **38**, 489 (2012).

[31] M. G. Cottam and D. J. Lockwood, *Light Scattering in Magnetic Solids* (Wiley, New York, 1986).

[32] P. A. Fleury and R. Loudon, Scattering of light by one- and two-magnon excitations, Phys. Rev. **166**, 514 (1968).

[33] N. J. Laurita, G. G. Marcus, B. A. Trump, J. Kindervater, M. B. Stone, T. M. McQueen, C. L. Broholm, and N. P. Armitage, Low-energy magnon dynamics and magneto-optics of the skyrmionic Mott insulator Cu_2OSeO_3, Phys. Rev. B **95**, 235155 (2017).

[34] Y. R. Shen and N. Bloembergen, Interaction between light waves and spin waves, Phys. Rev. **143**, 372 (1966).

[35] T. Nomura, X.-X. Zhang, S. Zherlitsyn, J. Wosnitza, Y. Tokura, N. Nagaosa, and S. Seki, Phonon Magnetochiral Effect, Phys. Rev. Lett. **122**, 145901 (2019).

[36] S. H. Liu, Magnetic excitations above the critical temperature, Phys. Rev. B **13**, 2979 (1976).

[37] E. J. Samuelsen and M. Melamud, Spin waves in antiferromagnets with alternating strong and weak coupling, J. Phys. C: Solid State Phys. **7**, 4314 (1974).

[38] R. B. Versteeg, I. Vergara, S. D. Schäfer, D. Bischoff, A. Aqeel, T. T. M. Palstra, M. Grüninger, and P. H. M. van Loosdrecht, Optically probed symmetry breaking in the chiral magnet Cu_2OSeO_3, Phys. Rev. B **94**, 094409 (2016).

[39] A. Compaan and H. J. Trodahl, Resonance Raman scattering in Si at elevated temperatures, Phys. Rev. B **29**, 793 (1984).

[40] See Supplemental Material at http://link.aps.org/supplemental/10.1103/PhysRevB.100.064401 for a comparison between the $\Delta S^z = \pm 1$ spin excitation spectral weight transients.

[41] N. Prasai, B. A. Trump, G. G. Marcus, A. Akopyan, S. X. Huang, T. M. McQueen, and J. L. Cohn, Ballistic magnon heat conduction and possible Poiseuille flow in the helimagnetic insulator Cu_2OSeO_3, Phys. Rev. B **95**, 224407 (2017).

[42] C. Kittel, Interaction of spin waves and ultrasonic waves in ferromagnetic crystals, Phys. Rev. **110**, 836 (1958).

[43] A. V. Kimel, R. V. Pisarev, J. Hohlfeld, and T. Rasing, Ultrafast Quenching of the Antiferromagnetic Order in $FeBO_3$: Direct Optical Probing of the Phonon-Magnon Coupling, Phys. Rev. Lett. **89**, 287401 (2002).

[44] P. G. Klemens, Anharmonic decay of optical phonons, Phys. Rev. **148**, 845 (1966).

[45] T. Ogasawara, K. Ohgushi, Y. Tomioka, K. S. Takahashi, H. Okamoto, M. Kawasaki, and Y. Tokura, General Features of Photoinduced Spin Dynamics in Ferromagnetic and Ferrimagnetic Compounds, Phys. Rev. Lett. **94**, 087202 (2005).

[46] L. Perfetti, P. A. Loukakos, M. Lisowski, U. Bovensiepen, H. Eisaki, and M. Wolf, Ultrafast Electron Relaxation in Superconducting $Bi_2Sr_2CaCu_2O_{8+\delta}$ by Time-Resolved Photoelectron Spectroscopy, Phys. Rev. Lett. **99**, 197001 (2007).

[47] See Supplemental Material at http://link.aps.org/supplemental/10.1103/PhysRevB.100.064401 for additional details on the three-temperature modeling.

[48] Z. Alpichshev, F. Mahmood, G. Cao, and N. Gedik, Confinement-Deconfinement Transition as an Indication of Spin-Liquid-Type Behavior in Na_2IrO_3, Phys. Rev. Lett. **114**, 017203 (2015).

[49] K. T. Law and P. A. Lee, $1T$-TaS_2 as a quantum spin liquid, Proc. Natl. Acad. Sci. USA **114**, 6996 (2017).